Implantable Nanosensors for Human Steroid Hormone Sensing In Vivo Using a Self#Templating Corona Phase Molecular Recognition

Citation: Lee, M. A., Wang, S., Jin, X., Bakh, N. A., Nguyen, F. T., Dong, J., Silmore, K. S., Gong, X., Pham, C., Jones, K. K., Muthupalani, S., Bisker, G., Son, M., Strano, M. S., Implantable Nanosensors for Human Steroid Hormone Sensing In Vivo Using a Self-Templating Corona Phase Molecular Recognition. Adv. Healthcare Mater. 2020, 9, 2000429.

As Published: http://dx.doi.org/10.1002/adhm.202000429

Publisher: Wiley

Persistent URL: https://hdl.handle.net/1721.1/140428

Version: Author's final manuscript: final author's manuscript post peer review, without publisher's formatting or copy editing

Implantable Nanosensors for Human Steroid Hormone Sensing In-Vivo using a Self-Templating Corona Phase Molecular Recognition

Michael A. Lee[1], Song Wang[1], Xiaojia Jin[1], Naveed Ali Bakh[1], Freddy T. Nguyen[1], Juyao Ivy Dong[1], Kevin Silmore[1], Xun Gong[1], Crystal Pham[1], Kelvin K. Jones[1], Sureshkumar Muthupalani[2], Gili Bisker[1,3], Manki Son[1], Michael S. Strano[1]

1. Department of Chemical Engineering, Massachusetts Institute of Technology, Cambridge, Massachusetts 02139, USA

2. Division of Comparative Medicine, Massachusetts Institute of Technology, Cambridge, Massachusetts 02139, USA

3. Department of Biomedical Engineering, Tel-Aviv University, Tel Aviv 6997801, Israel

Corresponding author: strano@mit.edu

Abstract

Dynamic measurements of steroid hormones *in vivo* is critical, but steroid sensing is currently limited by the availability of specific molecular recognition elements due to the chemical similarity of these hormones. In this work, we apply a new, self-templating synthetic approach using Corona Phase Molecular Recognition (CoPhMoRe) targeting the steroid family of molecules to produce near infrared fluorescent, implantable sensors. A key limitation of CoPhMoRe has been its reliance on library generation for sensor screening. We address this problem with a self-templating strategy of polymer design, using the examples of progesterone and cortisol sensing based on a styrene and acrylic acid copolymer library augmented with an acrylated steroid. The pendant steroid attached to the corona backbone is shown to self-template the phase, providing a unique CoPhMoRE design

This is the author manuscript accepted for publication and has undergone full peer review but has not been through the copyediting, typesetting, pagination and proofreading process, which may lead to differences between this version and the Version of Record. Please cite this article as doi: 10.1002/adhm.202000429.

strategy with high efficacy. The resulting sensors exhibit excellent stability and reversibility upon repeated analyte cycling. We show that molecular recognition using such constructs is viable even *in vivo* after sensor implantation into a murine model by employing a poly (ethylene glycol) diacrylate (PEGDA) hydrogel and porous cellulose interface to limit non-specific absorption. The results demonstrate that CoPhMoRe templating is sufficiently robust to enable a new class of continuous, *in vivo* biosensors.

Introduction

Steroid hormones act in numerous pathways dictating macromolecule metabolism,[1] reproduction,[2] inflammation,[3,4] among many others.[5] Dysfunction in steroid biochemistry is associated with various diseases,[6,7] though the exact mechanisms and use of steroids as biomarkers remain as topics of basic research.[8–12] Steroids are also regularly administered as therapeutics, requiring stringent dosages based on individual circumstances.[5] However, steroid signaling is unique in that it typically involves information carried as dynamic fluctuations in concentration, arguably of equal importance compared to concentration values reported from a typical biosensor[13]. Accordingly, the challenge for steroidal sensing is to create sensors that operate *in vivo*, capable of real-time measurements that report the temporal derivatives in concentration that promise to enhance medical diagnoses, elucidate mechanisms of disease, and augment therapies. Such prospective sensors for molecules as chemically similar as steroids (see Fig 1) require molecular recognition elements that remain stable within the harsh, complex implant environment. It remains a central question whether synthetic molecular recognition constructs can demonstrate and realize such stability. In this work, we address this challenge by developing a self-templating synthesis strategy for nanoparticle corona interfaces that enable the recognition of cortisol, progesterone and other steroids and steroid detection *in vivo* in mice.

Steroids regulate gene expression and a number of processes dictating physiological and pathological mechanisms. Key steroids include cortisol and progesterone. Cortisol plays a role in the stress response, macromolecular metabolism, and inflammation.[13] Cortisol is a key marker for various diseases, including Cushing's syndrome, Addison's disease, and various types of cancers.[14,15] Furthermore, cortisol has been studied as a biomarker for neuropsychiatric diseases, including major depression,[16] post-traumatic stress disorder,[17] and bipolar disorder.[18] A variety of assays are being developed for cortisol, including a recently reported point-of-care lateral flow assay utilizing aptamer-conjugated gold nanoparticles.[19] Progesterone dictates female sexual traits, including differentiation, menstruation, and pregnancy.[20] The dysregulation of progesterone pathways delineates classes of female cancers, including breast cancer.[21] These diseases are both deadly and widespread, occurring in approximately 1 in 8 women with a mortality rate of 40,000 per year.[22] Progesterone has also been a target for sensor development, including a recently reported amperometric sensor based on graphene covered tungsten trioxide nanoball electrodes.[23] In these cases, it is clear that steroid dynamics are a key indicator and symptom of dysregulation, further underscore the need for new analytical methods that operate continuously and *in-vivo*.

Additionally, measurements of steroids and their dynamics are central to therapeutic monitoring. For example, immunotherapies have emerged as promising candidates for the treatment of various types of cancer[24] but may induce undesired immune-related adverse events (IRAEs),[25] such as hepatitis, auto-immune diabetes, and hypothyroidism. In this case, a balance exists between tempering the immune response enough to resolve the IRAEs but not rendering the immunotherapy ineffective.[25] In the case of direct hormonal replacement, real time sensors can facilitate direct diurnal pattern control.[26] The current standard of measurement involves sampling blood and using

chromatography or immunoassays.[27] However, these methods are labor-intensive, costly, and lack temporal resolution.[28] Furthermore, in the case of cortisol, endogenous production involves a diurnal pattern, as well as stochastic release, such that single measurements fail to capture the complete profile.[13] For similar reasons, new point-of-care technologies based on molecular imprinting, aptamers, and antibodies, while valuable, do not address this specific problem of dynamic profiling.[28–32] Conversely, in the literature, there exist only a few examples *in vivo* steroid sensors, which have direct access to biological fluids. Takase et al. coupled cholesterol oxidase and an implantable electrode to monitor the cholesterol level in eye interstitial fluid in fish for 48 hours.[33] Cook measured cortisol in sheep and cattle using an electrochemical immunosensor implanted into the jugular veins.[34] Cook also used a microdialysis probe coupled to an immunosensor implanted in the amygdala of sheep to measure cortisol.[35] Sunwoo et al. implanted an enzyme-conjugated electrode into mice's adrenal glands to measure cortisol.[36]

In vivo steroid detection remains a challenging problem, but Corona Phase Molecular Recognition (CoPhMoRe) has emerged as a promising technique for recognizing complex analytes using nanosensors. In this technique, synthetic molecular recognition sites are created by non-covalently dispersing a nanoparticle 'transducer' such as a nIR fluorescent single walled carbon nanotube (SWNT) with polymers of specific composition. The corona necessarily excludes most molecules from interacting with the SWNT. Signal transduction is built into the nanoparticle as changes in the fluorescence spectrum as molecules bind to the SWNT surface. SWNT are particularly advantageous for long-term, spatiotemporal monitoring because they fluoresce in the tissue transparency window and do not photobleach.[37] Furthermore, the CoPhMoRe technique allows the selectivity of nanosensors to be engineered by modifying the suspending polymer. Previous CoPhMoRe sensors have included dopamine,[38,39] riboflavin, L-thryoxine, estradiol,[40] nitric oxide,[41,42] fibrinogen,[43] and

insulin.[44] The nitric oxide sensor has been used *in vivo* and shown to maintain its fluorescence stability over 400 days.[37]

Despite the success of CoPhMoRe for nanosensor development, a central limitation remains the reliance on a compositionally diverse library of corona phases to discover precise binding pockets for a target analyte. Synthesis of this library is often a technological hurdle that inhibits widespread use of the technique for a broad range of sensing problems. As an alternative, in this work, we demonstrate a polymer self-templating technique for CoPhMoRe that greatly reduces the requirements for an exploratory library. To date, CoPhMoRe sensors have been discovered empirically without a clear correlation between polymer dispersant structure and the target analyte.[45–47]. Here, we fabricated cortisol and progesterone sensors by utilizing corona phases incorporating template steroid molecules in a semi-rational manner. Furthermore, we demonstrate sensor selectivity for progesterone among not only molecules with wildly different structures but also among steroids themselves that have only slight variations on a structural motif, which has to date not been demonstrated. Last, a CoPhMoRe sensor based on synthetic polymers has not yet been taken from the first step of design to the end of an *in vivo* demonstration. In this work, we encapsulate our sensor into implantable hydrogel form factors and demonstrate sensitivity to local progesterone levels in the subcutaneous space of SKH1-E mice.

Experimental

Materials. Raw single wall carbon nanotubes (SWNT) produced by the HiPCO process were purchased from NanoIntegris and used without further processing (Batch HR27-104). Poly (ethylene glycol) diacrylate (PEGDA) (M_n = 8000) was purchased from Alfa Aesar. All other chemicals were purchased from Sigma Millipore.

Acrylation of Cortisol. Cortisol (2 grams, 1 equiv.) and triethylamine (850 mL, 1.1 equiv.) was dissolved in 50 mL tetrahydrofuran (THF). The solution was placed in an ice-bath under magnetic stirring. Acryloyl chloride (0.5 mL, 1.1 equiv.) diluted in THF at 10 vol% was added dropwise to the solution. The reaction proceeded at 0 ^{o}C for 1 hour and at room temperature thereafter for two days. The solution was decanted from the HCl-TEA salts. THF was removed by rotary evaporation. The product was reconstituted in 50 mL dichloromethane (DCM), washed thrice with 0.5 M HCl, twice with 5 wt% NaHCO3, and once with saturated aqueous NaCl. The solution was dried using anhydrous NaSO4. DCM was removed by rotary evaporation. 1.2 grams of product was obtained. The structure was confirmed using ^{1}H NMR using a Bruker AVANCE III -400 NMR Spectrometer (Figure S1).

Polymer Library Synthesis. Varying amounts of styrene (S), acrylic acid (AA), and acrylated cortisol (AC) monomers were dissolved in 10 mL 1,4-dioxane according to the specific polymer design (Figure S2, Table S1). MEHQ in acrylic acid and 4-*tert*-butylcatechol in styrene were removed by passing the reagents through columns packed with inhibitor removers. 2-(Dodecylthiocarbonothioylthio)-2-methylpropionic acid (1 equiv.) and 2,2'-Azobis(2-methylpropionitrile) (0.2 equiv.) were added to each reaction mixture. The solution was sparged with N_2 for 30 minutes and sealed in the nitrogen environment throughout the reaction. The reaction was conducted at 70 ^{o}C for 24 hours. After the reaction, the mixture was precipitated in 300 mL diethyl ether. The polymer was redissolved in THF and re-precipitated in diethyl ether twice more to remove unreacted monomer. The polymer was dried under vacuum for 3 days and stored at -20 ^{o}C until further use.

Polymer Characterization. NMR spectra were obtained by dissolving polymers at 30 mg/mL in methanol-d4. Molecular weight distributions were obtained using gel permeation chromatography on an Agilent Infinity 1260 equipped with a PL Aquagel-OH 30 column. The mobile phase was an aqueous solution of 0.2 M $NaNO_3$ and 0.01 M NaH_2PO_4 eluted at a flowrate of 0.5 mL/min. Samples were dissolved at 5 mg/mL, adjusted to pH 7, and filtered through a 0.22 um membrane prior to the run. The molar mass was calibrated against PEG standards ranging from 106 to 30,310 Da. FTIR spectra were measured from 500 – 4000 cm^{-1} with a Nicolet 4700 (Thermo Scientific) (Figure S4).

SWNT Suspension. In 5 mL of 1x PBS, 5 mg HiPCO SWNT and 50 mg of polymers were mixed. The solution was adjusted to a final pH of 7.4 using 2 M NaOH. The mixture was bath sonicated for 10 minutes and ultrasonicated using a 6 mm probe at a power of 10 W for 1 hour (QSonica). The resulting suspension was ultracentrifuged at 155,000 rcf for four hours. The top 80% of the suspension was reserved for further use, while the remaining 20% was discarded. Free polymer was removed from the suspension by dialysis against 1x PBS over 5 days using 100 kDa cutoff Float-a-Lyzer devices (Spectrum Labs) with buffer replacements thrice daily. UV-Vis-NIR absorption spectroscopy was used to confirm successful suspensions and obtain the mass concentration of the nanoparticles using an extinction coefficient of ε_{632} = 0.036 mg/(L cm).[48]

Sensor Screening. High throughput screening of the sensor library against the steroid panel was performed using a customized nIR microscope, which consists of a Zeiss Axio Vision inverted Microscope body with a 20x objective, coupled to an Acton SP2500 spectrometer and liquid nitrogen cooled InGaAs 1D detector (Princeton Instruments). In a 96 well plate, one SWNT sensor (1 mg/L) and one steroid (100 µM) were mixed in a final volume of 150 µL in 1x PBS with 2 vol% DMSO and incubated for 1 hour in each well. The samples were then illuminated by a 150 mW 785 nm

photodiode laser (B&W Tek Inc.), and fluorescence emission spectra were collected from 950 to 1250 nm. The fluorescence spectra were deconvoluted into individual peaks corresponding to single SWNT chiralities according to a previously reported algorithm (Figure S5).[40] Peak position and intensities of each sensor-steroid pair were compared to a sensor-blank control to calculate the sensor response. The most promising candidates were identified and studied further.

Molecular Dynamics (MD) Simulations. MD simulations were performed in GROMACS 4.6.5. Simulations were performed on (7,6) SWNT interacting with steroids and polymers containing various combinations of acrylic acid, styrene, and acrylated cortisol. SWNT, steroids, and polymers were created in Materials Studio 8.0. The OPLS-AA force field was used in the simulations. Parameters describing the bonds, bond angles, and dihedral angles of the monomers not in the original force field were obtained by using values from similar chemical structures already included (Supporting Information). SWNT were centered in a 10 nm x 10 nm x 4.8 nm box with the interacting molecule to be studied placed parallel to the SWNT. The box was hydrated using the TIP4P water model, and charges were neutralized using Na^+ counterions. Energy was minimized, and the system was equilibrated for 100 ps each under NVT and NPT ensembles. For steroids, a production run of 10 ns was conducted, while polymers were simulated using a production run of 200 ns. All simulations were performed at 300 K and with a 2 fs time step. Equilibration was confirmed by monitoring the polymer radius of gyration and the drift in the average Lennard-Jones potential.

Molecular Probe Adsorption (MPA) Surface Area. The free surface area of the polymer-wrapped SWNT was estimated using a molecular probe adsorption technique. Fluorescence calibration curves of riboflavin from 0 to 5 µM were measured using a Thermo VarioSkan Plate Reader. Riboflavin was excited at 460 nm, and emission were collected from 510 to 540 nm. Deflections of the riboflavin

fluorescence were taken in the presence of 10 mg/mL polymer and a solution of 10 mg/L SWNT with 10 mg/mL polymer. The surface area was estimated according to Park et al.[49]

Hydrogel Fabrication and Characterization. SWNT were encapsulated in a hydrogel matrix using a modified version of a previously reported protocol.[50] Briefly PEGDA (100 mg/L), dispersed SWNT (10 mg/L), and 2-hydroxy-4'-(2-hydroxyethoxy)-2-methylpriophenone (0.175 mg/mL) were mixed in 1x PBS. The mixture was placed into glass molds. After a 30-minute incubation in a nitrogen atmosphere, the molds were crosslinked under 365 nm ultraviolet light (UVP Blak-Ray XX-15BLB, 15 W) for 1 hour. The hydrogels were incubated in 1x PBS, with a replacement with fresh 1x PBS after 48 hours to remove unencapsulated SWNT and excess polymer.

Hydrogels were cut to 5 x 5 x 1 mm sections. Hydrogels were either used directly after fabrication or were placed into 6-8 kDa dialysis bags with a volume of 300 µL 1x PBS.

Fluorescence imaging on hydrogels were performed using a 2D InGaAs camera (Princeton Instruments) coupled to a Nikon AF Micro-Nikkor 60 mm 4/2.8D lens. The hydrogels were illuminated under a 785 nm Invictus laser (Kaiser). The optical window from 1075 – 1200 nm was monitored using a 1075 nm longpass filter and 1200 nm shortpass filter (Edmund Optics). To test progesterone responsivity, unencapsulated hydrogels were placed in 6-well plates and exposed to varying concentrations of progesterone. Hydrogels encapsulated in 6-8 kDa dialysis bags (Spectrum Labs) were imaged inside of transparent, 20 mL scintillation vials with 100 µM progesterone solution in 2% DMSO and 1x PBS.

Excitation-emission maps were constructed by tracking the fluorescence spectrum from 950 – 1250 nm while stepping the excitation from 500 – 800 nm in 5 nm increments. A 1 W broadband white laser (NKT Photonics) was coupled to a tunable filter with a 2 nm bandwidth (Photon Etc.) and fed to the aforementioned custom built NIR microscope array.

In vivo implantation and imaging. These procedures were reviewed and approved by the Committee on Animal Care at MIT. Prior to implantation, hydrogels were incubated in 2% DMSO and 1x PBS, with or without 100 µM progesterone for three hours. The hydrogels were then sterilized under 365 nm UV light (UVP Blak-Ray XX-15BLB, 15 W) for 10 minutes.

Female 7-week-old SKH-1E mice (Charles River Laboratory) were anesthetized under 2% isoflurane gas for 15 minutes. Once unresponsive to a toe pinch, the implantation site was sterilized using alternating washes with iopovidone and 70% ethanol repeated thrice. Hydrogels were placed subcutaneously in the dorsal side of the animal. The wound was closed with nylon sutures. Animals were imaged under 2% isoflurane using a 2D InGaAs camera coupled to a Nikon AF Micro-Nikkor 60 mm 4/2.8D lens, 1075 nm longpass filter, and 1200 nm shortpass filter. The mice were illuminated under a 785 nm Invictus laser dispersed over the surface of the animal to a power density of 10 mW/cm^2. After their experimental lifetime, mice were euthanized by CO_2 asphyxiation.

Statistical Analysis. Continuous variables are expressed as mean ± SEM (standard error). For normally distributed data sets with equal variances, two-tailed Student's t-test was carried out to determine significance. In all cases, significance was defined as $p \leq 0.05$. Statistical analysis was carried out using MATLAB R2018a.

Results and Discussion

Polymer Library Design. Central to the strategy of Corona Phase Molecular Recognition (CoPhMoRe) is a polymer pinned into a configuration onto a nanoparticle surface, which together act as a sensor transducer of molecular binding[38,40,43,44] (Figure 1a). In practice, a central limitation of CoPhMoRe has been its reliance on the construction of a library of corona phases from which recognition constructs can be screened. In this work, we discover and demonstrate a polymer self-templating technique shown to significantly reduce the library size needed to successfully apply CoPhMoRe. For self-templating, we attach a chemical appendage off of the polymer backbone, similar in molecular weight and structure to the target analyte to create a cavity within the corona similar in free volume and spatial polarity. As the appendage adsorbs and desorbs from the cavity, it exposes a high fidelity, reversible binding pocket within the corona phase for target recognition. We hypothesize that the appendage reversibly adsorbs while attached to the backbone, such that the vacancy produced is capable of recognizing molecules of similar size and shape. This templating could be considered a corona phase analog of molecular imprinting, except that the template remains bound to the backbone and no cross-linking is required.[51–57] An advantage is that the newly created binding site has direct access to the transducer, which can remain nanometer in scale. The bound appendage should be reversibly displaced upon addition of a more strongly adsorbing analyte. Using this strategy, we constructed two important steroid sensors: a cortisol sensor, P1-(6,5), and the progesterone sensor, P10-(7,6), as discussed in-depth below.

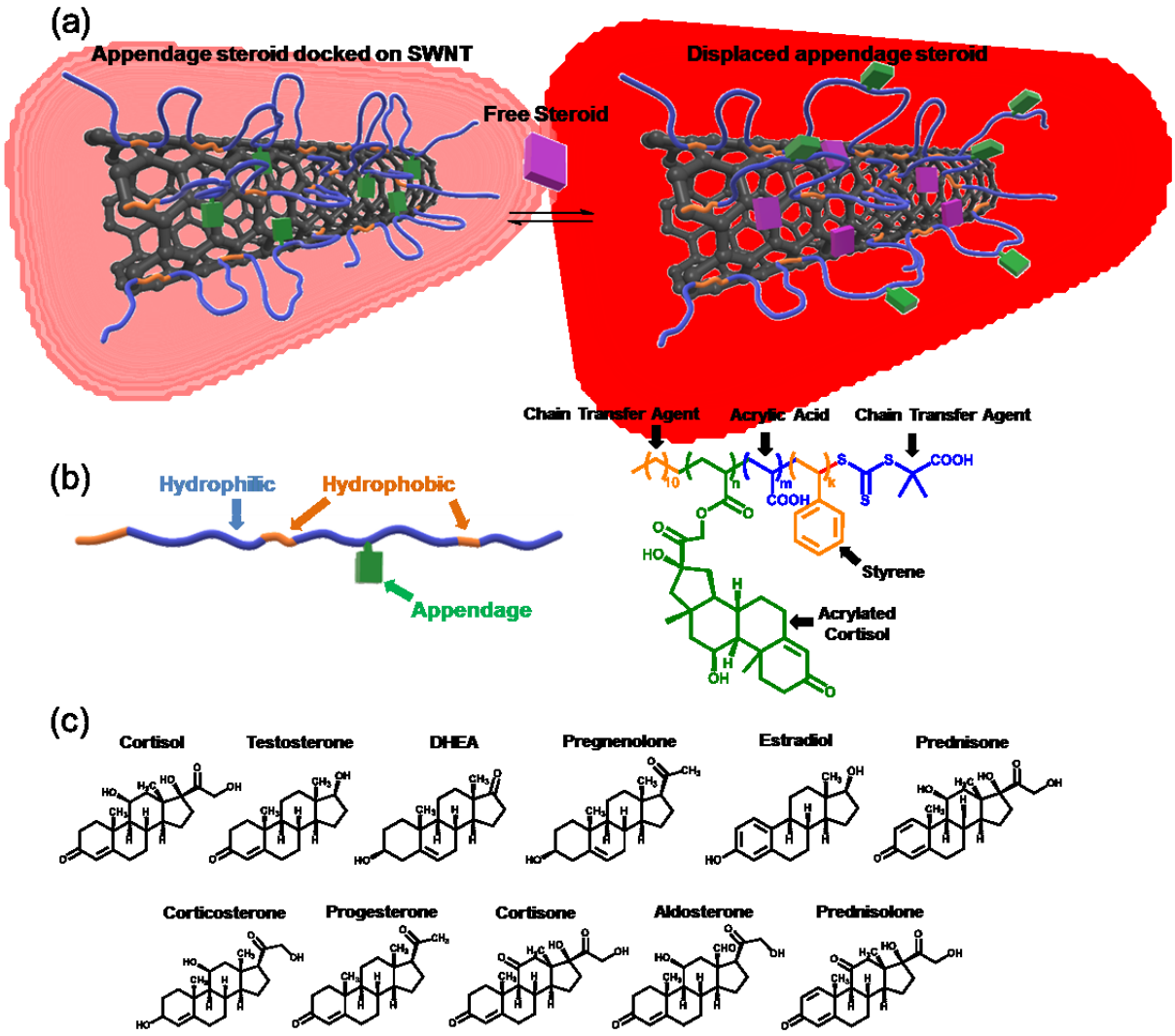

Figure 1: Semi-rational design for Corona Phase Molecular Recognition sensor for steroid hormone sensing. (a) Proposed mechanism of sensor. The initial configuration of the polymer on the SWNT involves charged hydrophilic groups (blue) extending out into aqueous solution and hydrophobic monomers (orange) anchoring the polymer non-covalently onto the SWNT. A template steroid molecule (green) is weakly bound to the SWNT, such that exogenously administered steroid molecules (magenta) will displace the appendage, resulting in a polymer configuration change and consequently change in SWNT fluorescence. (b) Polymers were composed of hydrophobic styrene monomers and alkyl chains (orange), hydrophilic acrylic acid monomers and carboxylic acid groups (blue), and acrylated cortisol (green). (c) Panel of steroid hormones used in the sensor screening, chosen for their physiological and therapeutic significance.

The corona phase library was generated using RAFT polymerization to generate random copolymers consisting of acrylic acid, styrene, and acrylated cortisol, the template. Acrylic acid, the hydrophilic unit, imparts colloidal stability at physiological pH. The hydrophobic styrene units anchor the polymer backbone onto the SWNT (Figure 1b). The unit composition of the polymers was varied to produce structurally diverse corona phases to sample a range of free-volumes and relative strengths

of dynamic binding/unbinding of the appendage. In total, we explore 80 unique corona phases in this work based on 16 polymer backbones to suspend five sets of SWNT chiralities grouped by emission maximum wavelengths: (8,3) and (6,5); (7,5); (10,2); (9,4) and (7,6); and (12,1). These SWNT span a range from 0.75 to 1.0 nm in diameter. These were tested against a panel of 11 steroids, chosen for their physiological and therapeutic significance (Figure 1c) with the resulting screening results in Figure 2.

The resulting heat map of binding shows several important trends with varying polymer composition (Figure 2a). A comparison between self-templated and non-templated polymers demonstrates increased affinity toward progesterone with greater appendage content in the polymers (Figure 2b-c), supporting this templating approach. A one-to-one correspondence between appendage structure and analyte selectivity is not observed. The appendage was based around the molecular structure of cortisol – which shares the three concatenated hexamer rings with one pentamer ring typical of steroids. The structural similarity between the steroid allow them to occupy the same type of cavity formed by the acrylated cortisol, while the polymeric unit together with the SWNT affect the binding affinity of the analytes toward the cavity. The resulting selectivity for progesterone suggests that it has a stronger affinity for the resulting cavity upon appendage desorption.

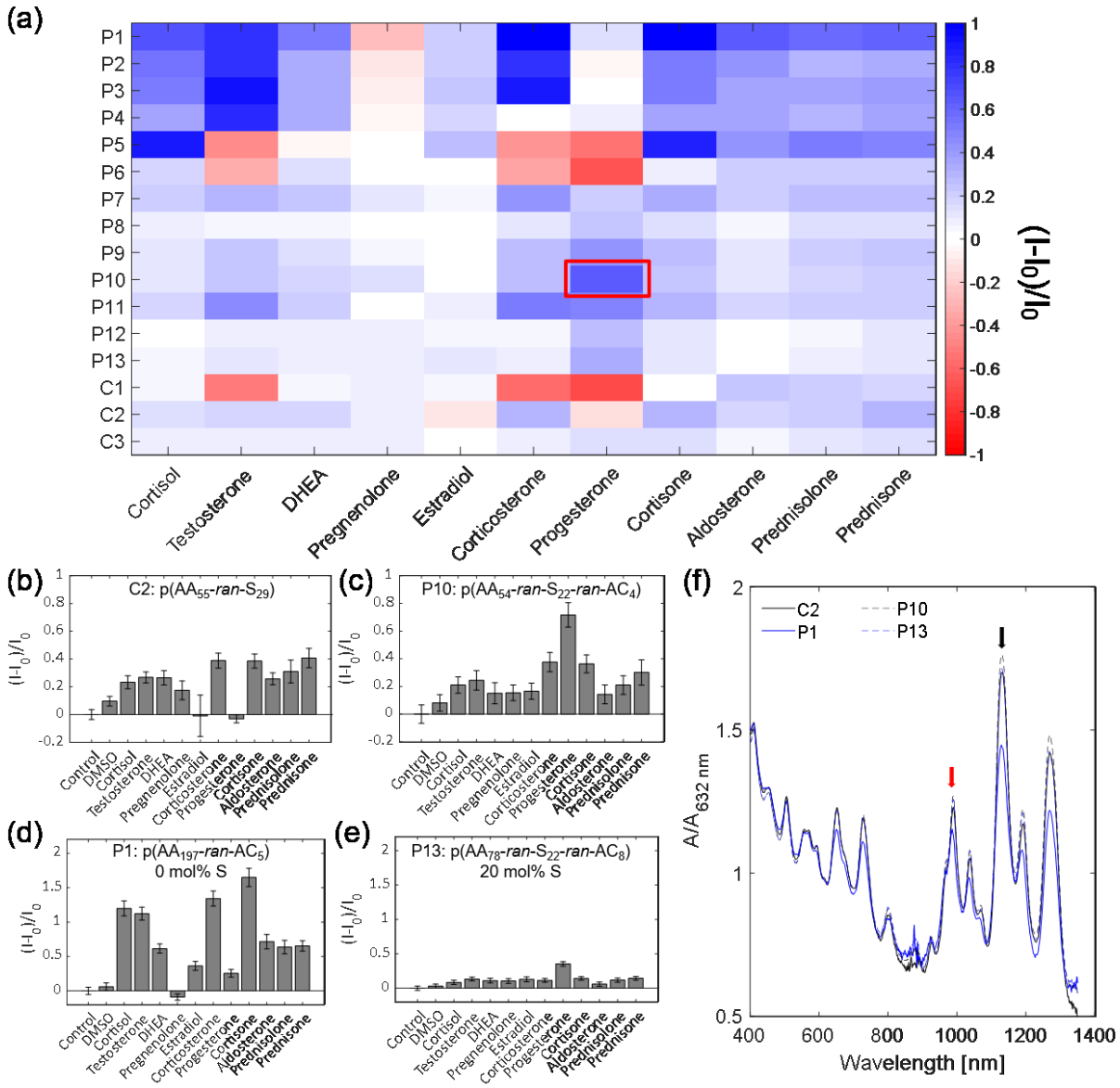

Figure 2: Summary of polymer library screening results. (a) Heat map showing the fractional fluorescence change, $(I-I_0)/I_0$, of the (9,4) and (7,6) chiralities of each member of the sensor library against 100 µM of each steroid in 2% DMSO and 1x PBS. Red denotes a fluorescence decrease, while blue indicates an increase. P indicates polymers with appendage steroids, while C denotes polymers without appendages. The selective response of P10-(7,6) is boxed in red. The full compositions of each polymer are given in Supporting Information. (b-e) Comparison of composite (9,4) and (7,6) fluorescence response of HiPCO SWNT wrapped with (b) C2, a polymer with 0 appendage units, versus (c) P10, a polymer with 4 appendage units. Increasing the number of appendage units while keeping the number of acrylic acid and styrene relatively fixed at approximately 55 and 25, respectively, increased progesterone selectivity and sensitivity. A polymer with (d) 0 mol% styrene, P1, exhibited higher steroid sensitivity but lower selectivity compared to a polymer with (e) higher styrene content at 20 mol%, P13 (data presented as mean ± SEM, n=3). (f) UV-Vis-NIR absorption spectrum of polymer-suspended HiPCO SWNT, indicating successful suspension of SWNT in the parameter space of the polymer library. The (9,4) and (7,6) channel is indicated with a black arrow arrow, while the red arrow indicates the (6,5) chirality.

Increasing styrene content systemically decreases nIR fluorescence response for the entire steroid library (Figure 2d-e). As an anchor, styrene may influence the responsivity in two ways: by sterically blocking the analyte from interacting with the SWNT and by constraining the mobility of the

anchored corona phase. Surface area measurements support styrene acting as a blocker, as P1-(6,5) with 0 mol% styrene and P10-(7,6) with 27.5 mol% styrene showed q/K_d values of 2.9×10^3 M^{-1} and 2.9×10^2 M^{-2}, respectively (Figure S12). Although styrene was designed primarily as an anchor, styrene may also dynamically desorb from SWNT and be stabilized in water by self-interactions with the amphiphilic polymer.

We examine two SWNT corona phases with moderately high selectivity: P1-(6,5) for cortisol and P10-(7,6) for progesterone. In this case, a sensor is considered selective to the steroid if the difference between the steroid response and average response if larger than three times of the standard error. Although other candidates such as P12-(7,6) and P13-(7,6) showed comparable selectivity towards progesterone, P10-(7,6) was chosen for further experiments due to its higher sensitivity toward progesterone. We ruled out aggregation and colloidal instability as alternative hypotheses for the observed selectivity, as the UV-Vis-NIR photoabsorption spectra of the sensors show well-resolved E_{11} and E_{22} transitions, consistent with colloidal dispersion (Figure 2f, S6-S7).[58] SWNT aggregation also causes nIR fluorescence quenching, as opposed to the observed fluorescence increases.[59]

P1-(6,5) consists of a (6,5) SWNT wrapped by p(AA_{197}-*ran*-AC_5) polymers and exhibits a 90% turn-on fluorescence response to cortisol (Figure 3a), whereas the magnitude of the second highest steroid response was 57% at 100 µM (Figure 3b). The sensor was exposed to varying cortisol concentrations, and the response was fit to the following functional form:

$$\frac{I - I_0}{I_0} = \beta \frac{C}{C + K_D} \quad (1)$$

Where I is the fluorescence intensity after steroid addition, I_0 is the original intensity, β is the proportionality factor between analyte occupancy and fluorescence intensity change, C is the steroid concentration, and K_D is the equilibrium dissociation constant (Figure 3c). A solution of 1 mg/L SWNT was responsive between 10 – 200 µM. With no inflection point (expected in a typical sigmoidal curve) observed in this concentration range, and extension beyond 200 µM limited by the low solubility of cortisol, calculation of a meaningful K_D value was precluded.

P10-(7,6), is selective to progesterone and is comprised of SWNT wrapped with p(AA_{53}-*ran*-S_{22}-*ran*-AC_4) polymers (Figure 3d). The response appears strongly chirality dependent, with the (10,2), (9,4), and (7,6) fluorescence peaks having the strongest response at 72% with the next highest steroid response inducing only a 38% fluorescence increase at 100 µM (Figure 3e). The calibration curve shows sensor responses between 5-100 µM and a K_D of 100 µM (Figure 3f). P10-(7,6) exhibited selectivity toward progesterone among steroids, other small molecules, and large molecular weight proteins (Figure 3g). Despite the common structural features among the steroids, no trends were observed when considering the oxidation state of each steroid, as well as the spatial distribution of oxygen groups on the backbone. Furthermore, we rule out the possibility of a non-specific hydrophobic interaction, as shown by sensor response vs. steroid logP value (Figure 3h).

These results show that the corona phase discriminates between steroids based on their specific molecular shape and chemical display. The curvature of the SWNT surface appears to influence the resulting corona phase binding, with the (10,2), (9,4), and (7,6) chiralities wrapped with P10 being the most sensitive to progesterone and the (6,5) chirality being non-selective (Figure 3i). A

fluorescence excitation-emission map taken before and after the addition of 100 µM confirms that these chiralities are the most sensitive to progesterone (Figure 3j-k).

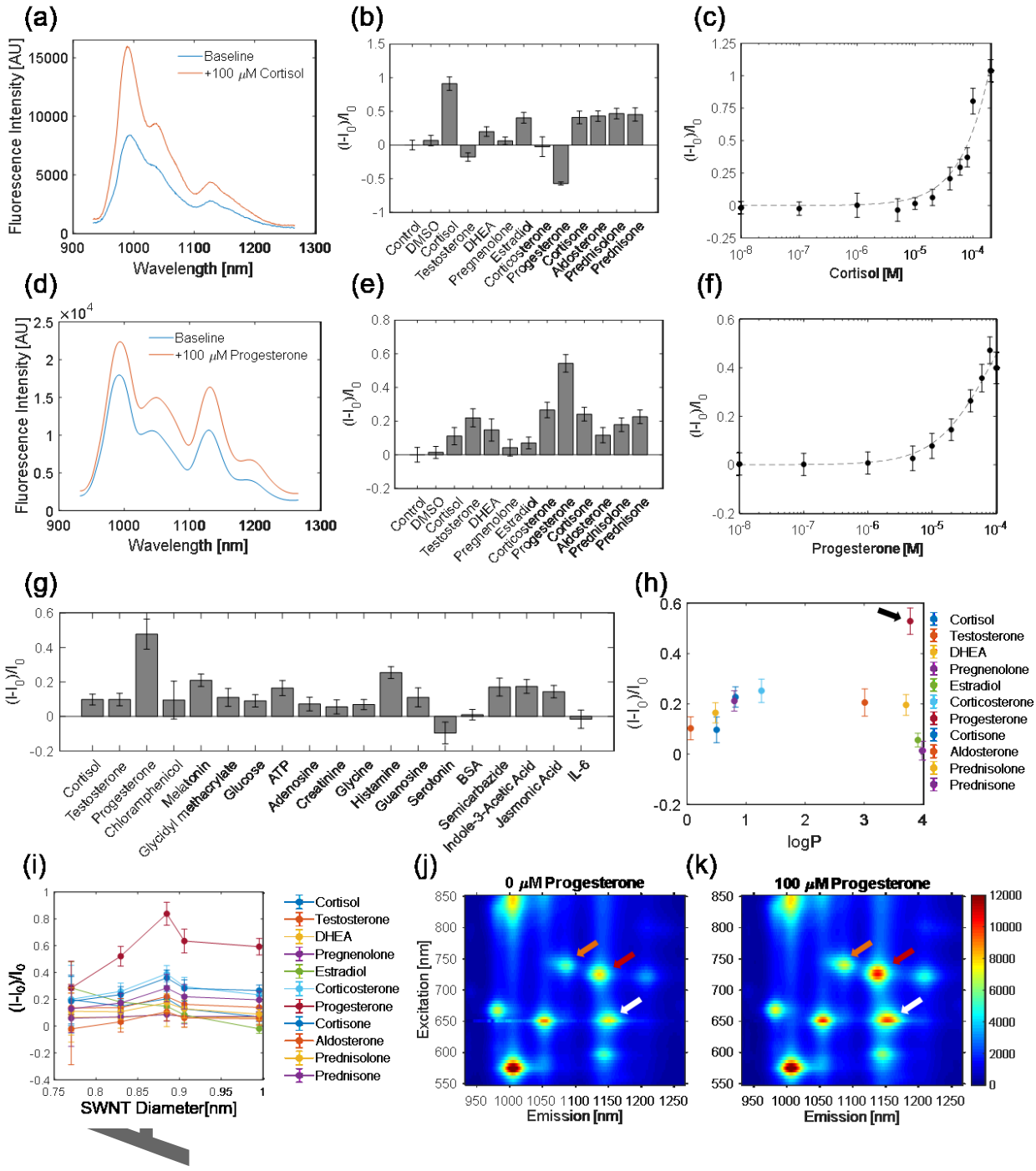

Figure 3: Sensor performance in solution phase. (a) The cortisol sensor consists of P1 polymer wrapped around (6,5) CoMoCAT SWNT, whose fluorescence increases in response to cortisol. (b) Cortisol induces approximately twice a change in fluorescence intensity magnitude versus the other steroids at the equivalent concentration of 100 µM (data

presented as mean ± SEM, n=3). (c) Calibration curve showing sensor sensitivity from 10 µM to 100 µM (data presented as mean ± SEM, n=3). (d) The progesterone sensor consists of P10 polymer wrapped around HiPCO SWNT, whose fluorescence increases in response to progesterone. (e) The progesterone sensor is selective towards progesterone over other steroids by a factor of 2, all tested at 100 µM (data presented as mean ± SEM, n=3). (f) The progesterone sensor has a detection range from 5 to 100 µM (data presented as mean ± SEM, n=3). (g) (9,4) and (7,6) SWNT wrapped with P10 exhibit selectivity toward progesterone even among other classes of small molecules and large proteins. (h) The progesterone sensing mechanism is not a simple hydrophobicity sensor, indicated by its sensor response relative to its partition coefficient. Progesterone is indicated by the black arrow. (i) The responsivity to each steroid of P10-wrapped SWNT depends on diameter, with an optimum SWNT diameter being observed for progesterone responsivity, as indicated by the arrow (data presented as mean ± SEM, n=3). (j-k) Excitation-emission plots of the progesterone sensor (j) before and (k) after the addition of 100 µM progesterone show that the (10,2), (9,4), and (7,6) chiralities are the most sensitive, as indicated by the arrows in orange, red, and white, respectively.

Molecular dynamics simulations were performed to further characterize the sensor-analyte interaction, and P10-(7,6) sensor for progesterone detection was chosen as a model system. In the absence of a corona, steroids adsorb onto bare SWNT to maximize the surface contact between its alkyl rings and the SWNT, while minimizing unfavorable repulsions due to protruding methyl groups and hydrophilic oxygen groups (Figure 4a). Short-range Lennard-Jones potentials did not vary significantly among steroids, with a range of -79 kJ/mol to -93 kJ/mol (Figure 4b). To quantify the relative energetic contributions of each monomer in P10 to the interaction with SWNT, simulations were conducted using with poly (acrylic acid)$_{20}$, poly(styrene)$_{20}$, and poly(acrylated cortisol)$_5$. The Lennard-Jones potential was -12.5 kJ/monomer, -17.3 kJ/monomer, and -81.4 kJ/monomer, for acrylic acid, styrene, and acrylated cortisol, respectively (Figure 4c). We observe that poly(acrylic acid) wraps around SWNT with the alkyl backbone adsorbed and its charged carboxylate groups pointing away from the SWNT (Figure 4d). Poly(styrene) interacts primarily through π-π stacking, with the phenyl rings interacting with SWNT in T-shaped, sandwich, and parallel-displaced configurations (Figure 4e). The relatively short distance (one carbon-carbon bond) between the phenyl group and alkyl backbone leads to inflexibility forcing some phenyl groups on the homopolymer to extend away from the SWNT. In random copolymers with fewer adjacent styrene residues, we expect this effect to be less pronounced. In the case of styrene not interacting with SWNT when incorporated into a random copolymer, the polymer itself is amphiphilic and can stabilize styrene residues through self-interactions. Poly(acrylated cortisol) wraps around the SWNT

to maximize binding with the steroidal rings, as described above (Figure 4f). Unlike styrene, however, there are three carbon-carbon bonds separating the rings from the alkyl chain, so all the monomers can wrap around the SWNT due to greater chain flexibility. When simulating the full P10 random copolymer, radial distribution functions confirm that on average styrene and acrylated cortisol equilibrate more closely to the SWNT compared to acrylic acid. (Figure 4g). These anchor-loop conformations were observed in simulation (Figure 4h) and are similar to those proposed in previous observations of CoPhMoRe[40,60].

The selectivity to small differences in steroid structure observed experimentally appear to be attributable to the overall conformation of the SWNT, P10, and steroid complexes. Acrylic acid is capable of hydrogen bonding with hydroxyls and carbonyl groups on steroids, with spacing controlled by polymer unit composition. Furthermore, the tethered appendages interact with the SWNT via hydrophobic interactions and with acrylic acids via H-bonding. Individual SWNT chiralities have different local curvature. Taken together, each corona should therefore be distinct and interact with each steroid with a different binding energy due to the distinct distribution of hydroxyl groups, carbonyls, and alkyl chains of each steroid, influencing selectivity. The emerging picture is one where the steroid occupies a binding pocket comprised of the SWNT, acrylic acid, styrene, and acrylated cortisol components (Figure 4i).

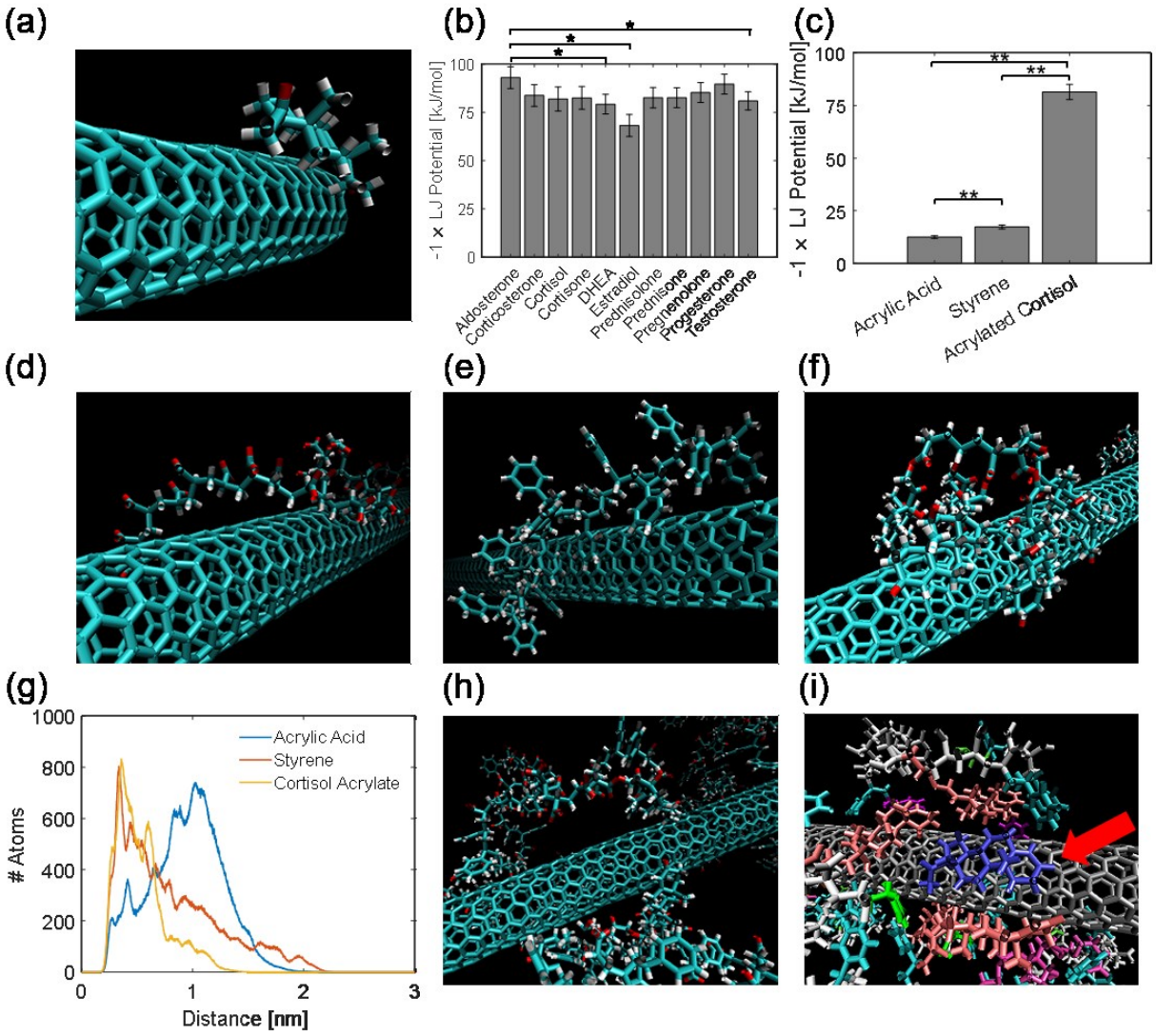

Figure 4: Molecular dynamics simulations to characterize SWNT corona. (a) Steroids adsorbed on bare (7,6) SWNT to maximize hydrophobic interactions while minimizing unfavorable steric interactions due to protruding methyl groups and contact with polar oxygen groups. (b) Short-range Lennard-Jones potential between steroids and bare (7,6) SWNT (data presented as mean ± SEM, n=3, P-values are calculated using two-tailed Students' t-test, *P<0.05, **P<0.005). (c) Short-range Lennard-Jones potential per monomer between (7,6) SWNT and poly (acrylic acid) with 20 units, poly(styrene) with 20 units, and poly (acrylated cortisol) with 5 units (data presented as mean ± SEM, n=3, P-values are calculated using two-tailed Students' t-test, *P<0.05, **P<0.005). (d-f) Snapshots of (d) poly (acrylic acid), (e) polystyrene, and (f) poly (acrylated cortisol) adsorbed onto (7,6) SWNT. (g) Radial distribution functions describing atom distance from surface of (7,6) SWNT for P10 adsorbed onto the SWNT surface. (h) Snapshot of P10 adsorbed on SWNT, demonstrating close proximity of styrene and acrylated cortisol and more distance acrylic acid from the SWNT surface. (i) A snapshot of progesterone (colored purple and indicated by arrow) occupying a binding site consisting of SWNT (silver), styrene (green), acrylic acid (white), and acrylated cortisol (peach).

Hydrogel Characterization. The progesterone sensor was chosen for further demonstration the potential *in vivo* application of the CoPhMoRe sensor because of its relative importance in the literature with fewer examples of sensors of this type[19,23,34,36]. In order to query the analyte data at

any time *in vivo,* a biocompatible and localizable sensor platform, such a hydrogel matrix, is required. Therefore, the progesterone sensor was tested in a variety of hydrogel materials (Figure 5a). Solution phase SWNT were mixed with the uncrosslinked polymers commonly used in hydrogels,[50] and the responses to 100 µM progesterone were measured. PEG had the least effect on baseline fluorescence, indicating the best preservation of the CoPhMoRe phase (Figure 5b). Furthermore, only the samples with PEG and poly(vinyl pyrrolidone) had identical responses to 100 µM progesterone as the sensor in 1x PBS (Figure 5c). Consequently, PEG was chosen as the encapsulating material for the progesterone sensor.

The functionality of the sensor in the hydrogel was verified through several tests. The hydrogel was exposed to alternating cycles of 0 and 100 µM progesterone in 1x PBS (Figure 5d). The hydrogel was kept stationary inside a well plate, while reservoirs of 0 and 100 µM progesterone were added and removed as needed. The hydrogel exhibited a stable and reversible response with a constant baseline, allowing. perturbations in fluorescence to be attributed to changes in analyte concentration. The fluorescence response was also calibrated against progesterone concentrations (Figure 5e). Additionally, the sensor still responded to 100 µM progesterone in 10% mouse serum with a magnitude of 12% (Figure 5f). By removing the progesterone solution and adding 10% mouse serum, the sensor reversibility was maintained with about 2% baseline drift. The lower response in serum suggests the presence of interfering molecules that reduce sensor sensitivity. Nevertheless, these interfering molecules may be avoided with strategic placement of the sensor. For example, implanting the hydrogel in the interstitial space as opposed to intravascularly avoids proteins such as albumin.[61] An excitation-emission map indicates that the most sensitive chiralities in the hydrogel were still the (10,2), (9,4), and (7,6) (Figure 5g).

The hydrogel-encapsulated SWNT exhibit a lower magnitude of response to progesterone at 30% versus the 60% observed in solution phase. Several contributions may exist. First, the crosslinked hydrogel matrix may reduce sensitivity by constraining the movements and reducing reconfiguration of the corona. Second, the free radicals produced during hydrogel fabrication may have chemically altered the suspending polymer on the SWNT, which were produced using RAFT polymerization and are living.

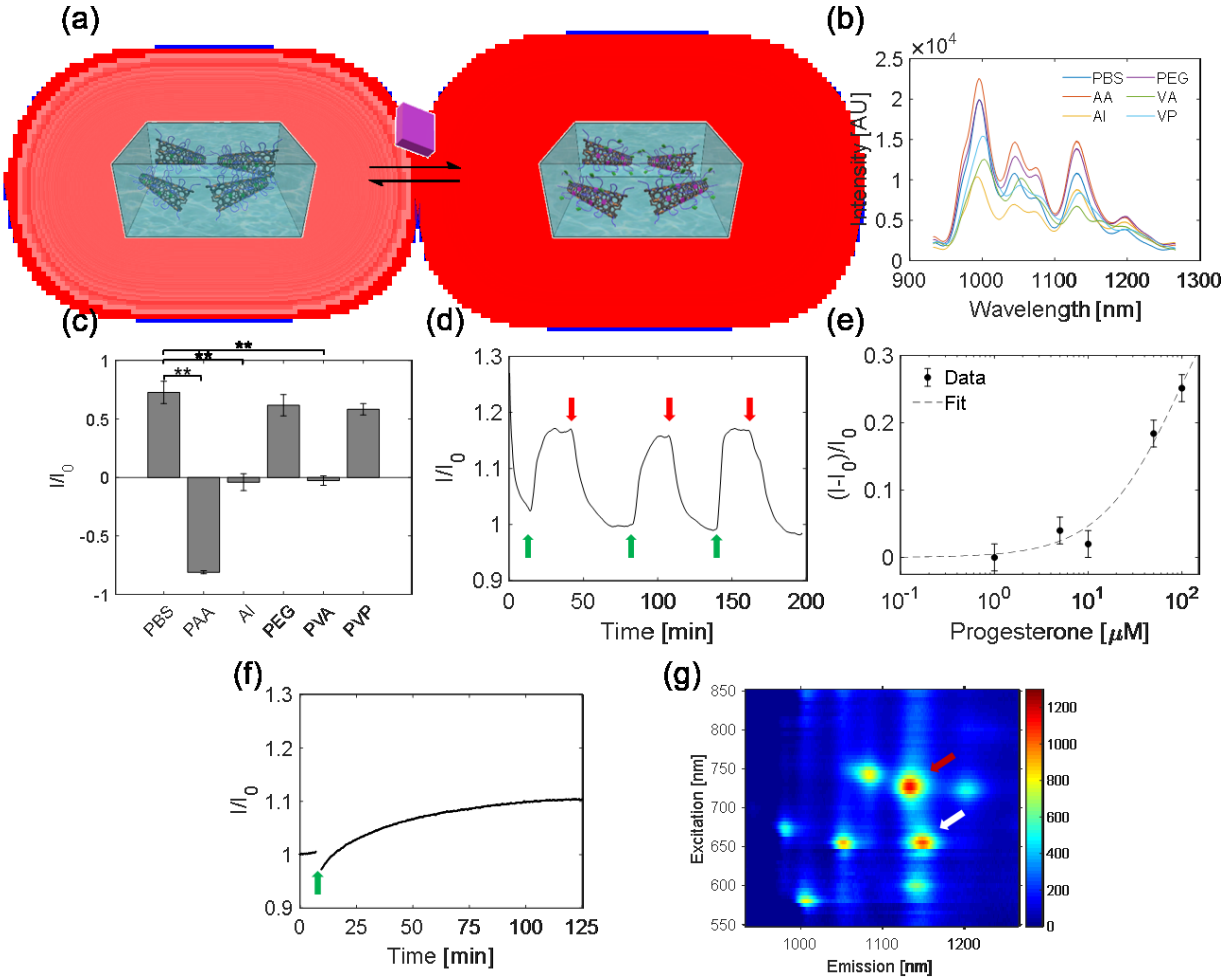

Figure 5: Hydrogel formulation, selection, and performance. (a) SWNT were encapsulated into PEGDA hydrogels, into which analytes diffuse and modulate fluorescence intensity. (b) Fluorescence spectrum of the progesterone sensor in 1x PBS and other commonly used hydrogel polymers before crosslinking. The degree of polymer interaction with SWNT can be seen by the shifting fluorescence spectrum. Among the different hydrogel components, PEG perturbed the sensor baseline fluorescence the least. (c) Sensor response to 100 µM when also incubated with hydrogel materials. Of the polymers tested, PEG and poly(vinyl pyrrolidone) preserved the sensor response compared to PBS (data presented as mean ± SEM, n=3, P-values are calculated using two-tailed Students' t-test, *P<0.05, **P<0.005). (d) Progesterone sensor encapsulated in PEGDA hydrogel exposed to varying cycles of 0 (red arrows) and 100 µM (green arrows) progesterone, showing a stable and reversible response of 18%. (e) Calibration curve of the progesterone sensor hydrogel (data presented as mean ± SEM, n=3). (f) The progesterone sensor hydrogel is functional in 10% mouse serum. (g) Excitation-

emission plots show that the (9,4) and (7,6) chiralities are most sensitive to progesterone, marked in red and white, respectively.

***In vivo* characterization.** As a proof of concept of *in vivo* measurements of progesterone with the CoPhMoRe sensor, we implanted the hydrogel subcutaneously into mice and monitored the sensor response over time. A dialysis bag (Figure 6a) with a molecular cutoff (MWCO) of 6-8 kDa was used to protect the sensor from interfering molecules and subsequent deactivation. We first measured the response profile of the dialysis bag encapsulated sensor to 100 µM progesterone *in vitro* (Figure 6b). The equilibrium response was 27% and leveled out after 3 hours.

We then implanted two hydrogels inside dialysis bags – one incubated in 100 µM progesterone and another incubated in 0 µM progesterone for three hours –simultaneously in multiple mice (Figure 6c). Analytes in interstitial fluid would be able to pass freely into and out of the hydrogel. The decrease in sensor fluorescence as progesterone diffuses away from the hydrogel was measured immediately after surgery. The sensor incubated in buffer served as a control to measure any signal perturbations due to the change in environment from buffer to interstitial fluid, as well as mouse movement. In each trial, the sensor incubated in progesterone showed a higher decrease in fluorescence relative to its paired control (Figure 6d). Over three mice, the sensor response was 22.1 ± 6.6%, and the control was 7.4 ± 3.7%. The difference was statistically significant with a one-tailed p-value of 0.016 (Figure 6e). The reversal monitoring demonstrates functionality of the sensor. H&E-stained tissue samples of the implant region taken after 28 days show the resolution of the acute inflammatory response and a well-defined epithelioid cap in both P10-(7,6) hydrogels and hydrogels without SWNT, indicating biocompatibility (Figure 6f-g).

To examine the necessity of the dialysis bag, we have also implanted hydrogels without dialysis bag and the sensors were found deactivated upon implantation in a time dependent manner (Figure 6h). Compared to non-implanted controls, hydrogels without dialysis bag implanted for two hours inside a mouse, extracted, and tested *in vitro* were completely insensitive to 100 µM progesterone. Conversely, hydrogels inside of 6-8 kDa dialysis bags still responded to 100 µM progesterone when extracted within 2 hours. After 24 hours in the mouse, the hydrogel was only partially deactivated. The delay of deactivation by using a 6-8 kDa dialysis bag permitted a 24-hour window, which further corroborated the *in vivo* test results described above.

The deactivation of the hydrogel suggests the presence of interfering molecules *in vivo* that either chemically alters or binds irreversibly to the CoPhMoRe site. FTIR measurements were performed on the hydrogels and no chemical functionalities of the bulk hydrogel material with implantation time was observed (Figure S13). Due to the low mass concentration, the SWNT and the suspending polymers are not visible in the IR spectra (Figure S14). However, the bulk hydrogel spectra before and after sensor deactivation are identical, indicating no chemical modification. One possible deactivation mechanism involves clogging of the hydrogel pores with interfering molecules, leading to regions of physically inaccessible and therefore chemically insensitive SWNT. Given that the sensor functions in mouse serum, the interferents may be inflammatory molecules released at the implantation site during surgery, such as cytokines, protein fragments, reactive oxygen and nitrogen species, etc.[62] Furthermore, the deactivation with the dialysis bag over 24 hours suggest that at least one of the interferents has a molar mass on the order of 5 kDa. Precise identification of the interferents will be the subject of future work. Accordingly, the sensor formulation will be modified to mitigate the deactivation, as well as to decrease the limit of detection to target physiological values of progesterone. Physiological concentrations of cortisol and progesterone in typical people

are lower than the dynamic range of the sensor. Cortisol exists between 0-500 nM,[13] while progesterone can range from 0 to 800 nM depending on the status of pregnancy.[63,64]

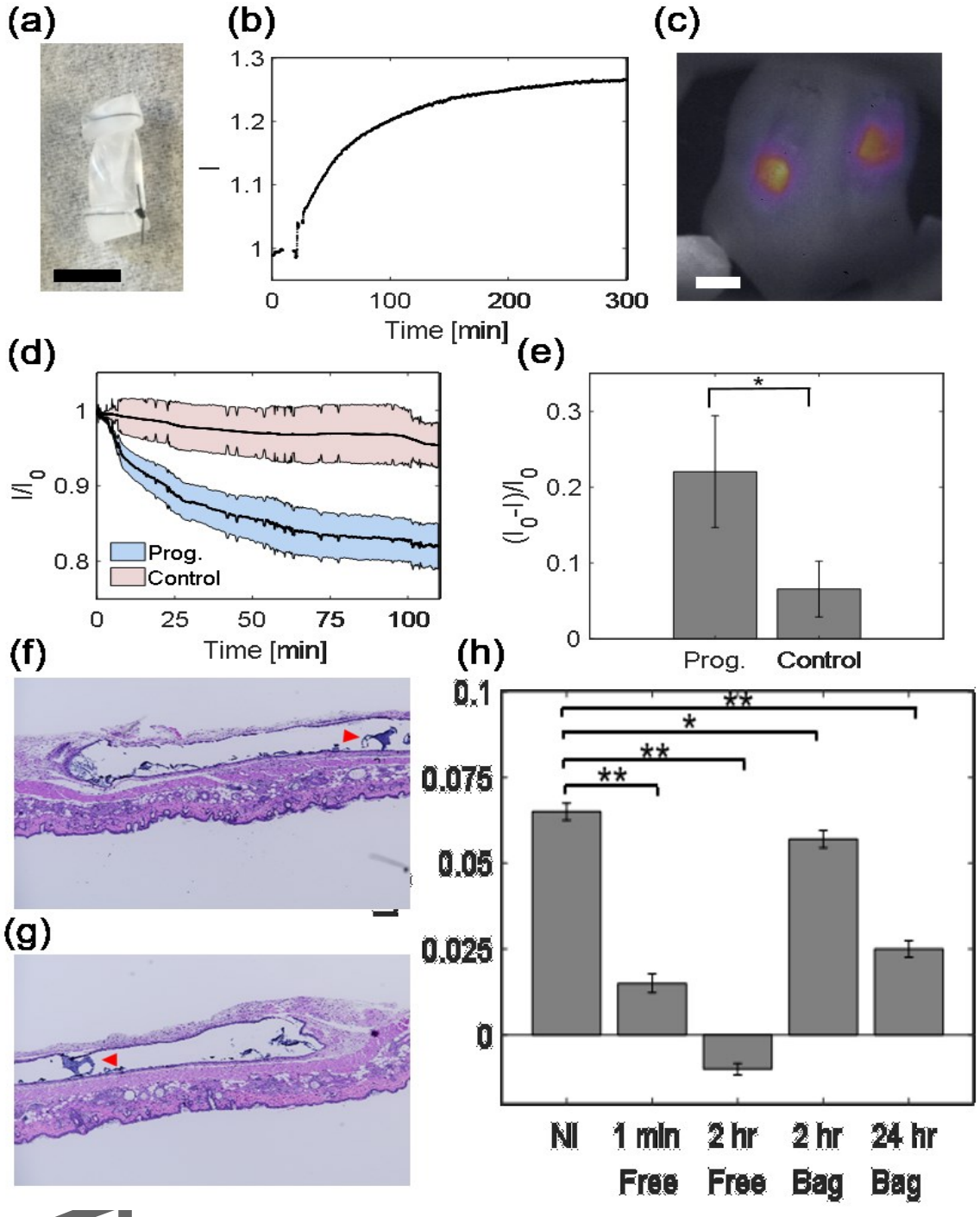

Figure 6 : Proof of concept of in vivo steroid sensor monitoring progesterone. (a) Hydrogels inserted into 6-8 kDa dialysis bags (scale = 5 mm). (b) In vitro response of hydrogel inside of dialysis bags to 100 µM progesterone. (c) Two hydrogels inside of dialysis bags implanted simultaneously in the dorsal subcutaneous space of SKH1-E mice (scale = 10 mm). One dialysis bag was incubated in 100 µM progesterone, while the other was incubated in the control buffer. (d) The dialysis bag incubated in progesterone shows a higher magnitude fluorescence decrease over the control bag, as progesterone

diffuses outside of the sensor hydrogel. The colored area represents the S.E.M. (n=3). (e) The trend was reproducible in 3 mice, with p < 0.02 (data presented as mean ± SEM, n=3, P-values are calculated using one-tailed Students' t-test, *P<0.05, **P<0.005). (f-g) H&E stained tissue samples surrounding the implant region of (f) P10-(7,6) hydrogels and (g) hydrogels without SWNT after 28 days of implantation and imaged at 4x magnification. Both hydrogels show the resolution of the acute inflammatory response and a well-defined epithelioid cap indicating healing. The hydrogels are marked with red arrows. (h) Response of sensor hydrogels to 100 μM progesterone outside of mice. The hydrogels were implanted subcutaneously either directly or inside of 6-8 kDa dialysis bags for varying durations of time and subsequently extracted. NI indicates a non-implanted control. Direct implantation leads to deactivation over time, while the use of a dialysis bag slows the deactivation (data presented as mean ± SEM, n=3, P-values are calculated using two-tailed Students' t-test, *P<0.05, **P<0.005).

Conclusions and Future Work

In total, these experiments demonstrate both the feasibility of the sensor development process that starts with CoPhMoRe library discovery, encapsulation into a biocompatible vehicle, and *in vivo* measurement. In its current form, the sensor has two central limitations for *in vivo* applications. First, the limit of detection is in the μM range, while steroids exist at nM levels in the body. Second, even among the most selective sensors in this study still had some cross-reactivity with other steroids. In future work, selectivity and sensitivity might be improved by exploring several strategies. In this work, we only utilized acrylated cortisol as a template. However, the design space can be expanded substantially by exploring other template steroids, differing in both base steroid and chemical modifications. Additionally, given the chirality-dependent nature of the sensor response and the high bandwidth of SWNT emission peaks, we were limited to some extent by utilizing SWNT that were a mix of various chiralities. As the field of SWNT purification continues to improve, we can increase our sensitivity by utilizing purer samples of SWNT with the chiralities of interest. Furthermore, we utilized a PEG hydrogel in this study. Another possible strategy is to employ more complex hydrogels that could increase the local concentration of steroid around the sensor. Some possible components include molecularly imprinted polymers that have been demonstrated to have an affinity for steroids. To permit long-term monitoring of steroid, the sensor deactivation mechanism will be elucidated, and interfering molecules will be identified. In this way, several unique sensors for a range of bioanalytes can be constructed to enable multiplexed biomarker measurements to compose a comprehensive evaluation of an individual's health.

Acknowledgments

This research was supported by the King Abdullah University of Science & Technology (OSR-2015 Sensors 2707). FTN is supported by the Arnold and Mabel Beckman Foundation through the Arnold O. Beckman Postdoctoral Fellowship.

Author Contributions

MAL and MSS formulated the experimental design and concepts. MAL and SW designed the polymer library, performed the synthesis, and performed sensor characterization. MAL, NAB, XJ, CP, and KKJ produced and characterized hydrogels. FTN aided in optical instrumentation. MAL performed the animal experiments, XG aided in the image analysis, and SM performed the histological analysis. MAL, JID, and KSS performed the molecular simulations. MS and GHB contributed to data interpretation.

Competing financial interests

The authors declare no competing financial interest.

References

1. Fernandez-Real, J.-M., Pugeat, M., Emptoz-Bonneton, A. & Ricart, W. Study of the effect of changing glucose, insulin, and insulin-like growth factor-I levels on serum corticosteroid binding globulin in lean, obese, and obese subjects with glucose intolerance. *Metabolism* **50**,

1248–1252 (2001).

2. Nock, B. & Feder, H. H. Neurotransmitter modulation of steroid action in target cells that mediate reproduction and reproductive behavior. *Neurosci. Biobehav. Rev.* **5**, 437–447 (1981).

3. Barnes, P. J., Adcock, I., Spedding, M. & Vanhoutte, P. M. Anti-inflammatory actions of steroids: molecular mechanisms. *Trends Pharmacol. Sci.* **14**, 436–441 (1993).

4. Sapolsky, R. M., Romero, L. M. & Munck, A. U. How Do Glucocorticoids Influence Stress Responses? Integrating Permissive, Suppressive, Stimulatory, and Preparative Actions. *Endocr. Rev.* **21**, 55–89 (2000).

5. Litwack, G. Steroid Hormones. in *Human Biochemistry* (ed. Litwack, G. B. T.-H. B.) 467–506 (Academic Press, 2018). doi:https://doi.org/10.1016/B978-0-12-383864-3.00016-8

6. Honour, J. W. Diagnosis of Diseases of Steroid Hormone Production, Metabolism and Action. *J. Clin. Res. Pediatr. Endocrinol.* **1**, 209–226 (2009).

7. Miller, W. L. & Auchus, R. J. The Molecular Biology, Biochemistry, and Physiology of Human Steroidogenesis and Its Disorders. *Endocr. Rev.* **32**, 81–151 (2011).

8. Hartmann, K. *et al.* Molecular Actions of Glucocorticoids in Cartilage and Bone During Health, Disease, and Steroid Therapy. *Physiol. Rev.* **96**, 409–447 (2016).

9. Almeida, M. *et al.* Estrogens and Androgens in Skeletal Physiology and Pathophysiology. *Physiol. Rev.* **97**, 135–187 (2016).

10. Dobruch, J. *et al.* Gender and Bladder Cancer: A Collaborative Review of Etiology, Biology, and Outcomes. *Eur. Urol.* **69**, 300–310 (2016).

11. Kim, C. *et al.* A Review of the Relationships Between Endogenous Sex Steroids and Incident Ischemic Stroke and Coronary Heart Disease Events. *Current Cardiology Reviews* **11**, 252–260

12. Bansal, R. & Singh, R. Exploring the potential of natural and synthetic neuroprotective steroids against neurodegenerative disorders: A literature review. *Med. Res. Rev.* **38**, 1126–1158 (2018).

13. Lee, M. A., Bakh, N., Bisker, G., Brown, E. N. & Strano, M. S. A Pharmacokinetic Model of a Tissue Implantable Cortisol Sensor. *Adv. Healthc. Mater.* **5**, 3004–3015 (2016).

14. Gupta, S. K. & Dubé, M. P. Exogenous cushing syndrome mimicking human immunodeficiency virus lipodystrophy. *Clin. Infect. Dis.* **35**, E69-71 (2002).

15. Napier, C. & Pearce, S. H. S. Current and emerging therapies for Addison's disease. *Curr. Opin. Endocrinol. Diabetes Obes.* **21**, 147–153 (2014).

16. LeMoult, J. & Joormann, J. Depressive rumination alters cortisol decline in Major Depressive Disorder. *Biol. Psychol.* **100**, 50–55 (2014).

17. Yahyavi, S. T., Zarghami, M., Naghshvar, F. & Danesh, A. Relationship of cortisol, norepinephrine, and epinephrine levels with war-induced posttraumatic stress disorder in fathers and their offspring . *Revista Brasileira de Psiquiatria* **37**, 93–98 (2015).

18. Steen, N. E. *et al.* Altered systemic cortisol metabolism in bipolar disorder and schizophrenia spectrum disorders. *J. Psychiatr. Res.* **52**, 57–62 (2014).

19. Dalirirad, S. & Steckl, A. J. Aptamer-based lateral flow assay for point of care cortisol detection in sweat. *Sensors Actuators B Chem.* **283**, 79–86 (2019).

20. Bouchard, P. Progesterone and the progesterone receptor. *J. Reprod. Med.* **44**, 153–157 (1999).

21. Dinny Graham, J. & Clarke, C. L. Physiological action of progesterone in target tissues. *Endocrine Reviews* (1997). doi:10.1210/er.18.4.502

22. Siegel, R. L., Miller, K. D. & Jemal, A. Cancer statistics, 2018. *CA. Cancer J. Clin.* (2018). doi:10.3322/caac.21442

23. Govindasamy, M. *et al.* Ultrasound-assisted synthesis of tungsten trioxide entrapped with graphene nanosheets for developing nanomolar electrochemical (hormone) sensor and enhanced sensitivity of the catalytic performance. *Ultrason. Sonochem.* **56**, 134–142 (2019).

24. Sharma, P. & Allison, J. P. The future of immune checkpoint therapy. *Science (80-.).* **348**, 56 LP – 61 (2015).

25. Michot, J. M. *et al.* Immune-related adverse events with immune checkpoint blockade: a comprehensive review. *Eur. J. Cancer* **54**, 139–148 (2016).

26. Bornstein, S. R. *et al.* Diagnosis and Treatment of Primary Adrenal Insufficiency: An Endocrine Society Clinical Practice Guideline. *J. Clin. Endocrinol. Metab.* **101**, 364–389 (2016).

27. Gatti, R. *et al.* Cortisol assays and diagnostic laboratory procedures in human biological fluids. *Clin. Biochem.* **42**, 1205–1217 (2009).

28. Kaushik, A., Vasudev, A., Arya, S. K., Pasha, S. K. & Bhansali, S. Recent advances in cortisol sensing technologies for point-of-care application. *Biosens. Bioelectron.* **53**, 499–512 (2014).

29. Singh, A., Kaushik, A., Kumar, R., Nair, M. & Bhansali, S. Electrochemical Sensing of Cortisol: A Recent Update. *Appl. Biochem. Biotechnol.* **174**, 1115–1126 (2014).

30. Klouda, J., Barek, J., Nesměrák, K. & Schwarzová-Pecková, K. Non-Enzymatic Electrochemistry in Characterization and Analysis of Steroid Compounds. *Crit. Rev. Anal. Chem.* **47**, 384–404 (2017).

31. Gugoasa, L. A. & Staden, R.-I. S. Advanced Methods for the Analysis of Testosterone. *Current Medicinal Chemistry* **25**, 4037–4049

32. Campuzano, S., Yánez-Sedeño, P. & Pingarrón, J. M. Electrochemical bioaffinity sensors for

salivary biomarkers detection. *TrAC Trends Anal. Chem.* **86**, 14–24 (2017).

33. Takase, M., Murata, M., Hibi, K., Huifeng, R. & Endo, H. Development of mediator-type biosensor to wirelessly monitor whole cholesterol concentration in fish. *Fish Physiol. Biochem.* **40**, 385–394 (2014).

34. Cook, C. J. Real-time measurements of corticosteroids in conscious animals using an antibody-based electrode. *Nat. Biotechnol.* **15**, 467–471 (1997).

35. Cook, C. J. Glucocorticoid feedback increases the sensitivity of the limbic system to stress. *Physiol. Behav.* **75**, 455–464 (2002).

36. Sunwoo, S. H. *et al.* Chronic and acute stress monitoring by electrophysiological signals from adrenal gland. *Proc. Natl. Acad. Sci.* **116**, 1146 LP – 1151 (2019).

37. Iverson, N. M. *et al.* In vivo biosensing via tissue-localizable near-infrared-fluorescent single-walled carbon nanotubes. *Nat. Nanotechnol.* **8**, 873–880 (2013).

38. Kruss, S. *et al.* Neurotransmitter detection using corona phase molecular recognition on fluorescent single-walled carbon nanotube sensors. *J. Am. Chem. Soc.* **136**, 713–724 (2014).

39. Kruss, S. *et al.* High-resolution imaging of cellular dopamine efflux using a fluorescent nanosensor array. *Proc. Natl. Acad. Sci.* **114**, 1789–1794 (2017).

40. Zhang, J. *et al.* Molecular recognition using corona phase complexes made of synthetic polymers adsorbed on carbon nanotubes. *Nat. Nanotechnol.* **8**, 959–68 (2013).

41. Zhang, J. Q. *et al.* Single Molecule Detection of Nitric Oxide Enabled by d(AT)(15) DNA Adsorbed to Near Infrared Fluorescent Single-Walled Carbon Nanotubes. *J. Am. Chem. Soc.* **133**, 567–581 (2011).

42. Giraldo, J. P. *et al.* A Ratiometric Sensor Using Single Chirality Near-Infrared Fluorescent Carbon Nanotubes: Application to in Vivo Monitoring. *Small* **11**, 3973–3984 (2015).

43. Bisker, G. *et al.* Protein-targeted corona phase molecular recognition. *Nat. Commun.* **7**, 1–14 (2016).

44. Bisker, G. *et al.* Insulin Detection Using a Corona Phase Molecular Recognition Site on Single-Walled Carbon Nanotubes. *ACS Sensors* **3**, 367–377 (2018).

45. Bisker, G. *et al.* A mathematical formulation and solution of the CoPhMoRe inverse problem for helically wrapping polymer corona phases on cylindrical substrates. *J. Phys. Chem. C* **119**, 13876–13886 (2015).

46. Salem, D. P. *et al.* Chirality dependent corona phase molecular recognition of DNA-wrapped carbon nanotubes. *Carbon N. Y.* **97**, 147–153 (2016).

47. Salem, D. P. *et al.* Ionic Strength-Mediated Phase Transitions of Surface-Adsorbed DNA on Single-Walled Carbon Nanotubes. *J. Am. Chem. Soc.* **139**, 16791–16802 (2017).

48. Zhang, J. *et al.* A Rapid, Direct, Quantitative, and Label-Free Detector of Cardiac Biomarker Troponin T Using Near-Infrared Fluorescent Single-Walled Carbon Nanotube Sensors. *Adv. Healthc. Mater.* (2014). doi:10.1002/adhm.201300033

49. Park, M. *et al.* Measuring the Accessible Surface Area within the Nanoparticle Corona Using Molecular Probe Adsorption. *Nano Lett.* **19**, 7712–7724 (2019).

50. Iverson, N. M. *et al.* Quantitative tissue spectroscopy of near infrared fluorescent nanosensor implants. *J. Biomed. Nanotechnol.* **12**, 1035–1047 (2016).

51. Hishiya, T., Shibata, M., Kakazu, M., Asanuma, H. & Komiyama, M. Molecularly Imprinted Cyclodextrins as Selective Receptors for Steroids. *Macromolecules* **32**, 2265–2269 (1999).

52. Manickam, P., Pasha, S. K., Snipes, S. A. & Bhansali, S. A Reusable Electrochemical Biosensor for Monitoring of Small Molecules (Cortisol) Using Molecularly Imprinted Polymers. *J. Electrochem. Soc.* **164**, B54–B59 (2017).

53. Farber, S., Green, B. S. & Domb, A. J. Selective 17-β-estradiol molecular imprinting. *J. Polym. Sci. Part A Polym. Chem.* **47**, 5534–5542 (2009).

54. Özgür, E. *et al.* A new molecular imprinting-based mass-sensitive sensor for real-time detection of 17β-estradiol from aqueous solution. *Environ. Prog. Sustain. Energy* **32**, 1164–1169 (2012).

55. Kellens, E. *et al.* Improved Molecular Imprinting Based on Colloidal Particles Made from Miniemulsion: A Case Study on Testosterone and Its Structural Analogues. *Macromolecules* **49**, 2559–2567 (2016).

56. Ramström, O., Ye, L. & Mosbach, K. Artificial antibodies to corticosteroids prepared by molecular imprinting. *Chem. Biol.* **3**, 471–477 (1996).

57. Cheong, S. H. *et al.* Testosterone Receptor Binding Mimic Constructed Using Molecular Imprinting. *Macromolecules* **30**, 1317–1322 (1997).

58. Choi, J. H. & Strano, M. S. Solvatochromism in single-walled carbon nanotubes. *Appl. Phys. Lett.* **90**, (2007).

59. Weisman, R. B. Chapter 5 Optical spectroscopy of single-walled carbon nanotubes. in *Carbon Nanotubes: Quantum Cylinders of Graphene* (eds. Saito, S. & Zettl, A. B. T.-C. C. of C. M. S.) **3**, 109–133 (Elsevier, 2008).

60. Ulissi, Z. W., Zhang, J., Sresht, V., Blankschtein, D. & Strano, M. S. 2D Equation-of-State Model for Corona Phase Molecular Recognition on Single-Walled Carbon Nanotube and Graphene Surfaces. *Langmuir* **31**, 628–636 (2015).

61. Adamczyk, Z., Nattich-Rak, M., Dąbkowska, M. & Kujda-Kruk, M. Albumin adsorption at solid substrates: A quest for a unified approach. *J. Colloid Interface Sci.* **514**, 769–790 (2018).

62. Dang, T. T., Nikkhah, M., Memic, A. & Khademhosseini, A. Polymeric Biomaterials for

Implantable Prostheses. in *Natural and Synthetic Biomedical Polymers* (eds. Kumbar, S. G., Laurencin, C. T. & Deng, M. B. T.-N. and S. B. P.) 309–331 (Elsevier, 2014). doi:https://doi.org/10.1016/B978-0-12-396983-5.00020-X

63. Dunning, M. B. & Fischbach, F. *Nurses' Quick Reference to Common Laboratory & Diagnostic Tests*. (2010).

64. Booth, M. & El Garf, T. A. R. Plasma Progesterone Concentration During the Third Trimester of Diabetic Pregnancy. *BJOG An Int. J. Obstet. Gynaecol.* **81**, 768–776 (1974).

A hydrogel-encapsulated carbon nanotube biosensor detects the steroid hormone progesterone in the subcutaneous space of mice. The biosensor is synthesized using a polymeric, self-templated Corona Phase Molecular Recognition (CoPhMoRe) strategy, which is adaptable to target other steroid hormones, including the stress hormone cortisol. The progesterone and cortisol biosensors show selectivity among both other similarly-structured steroids, as well as a larger panel of various biomolecules, opening further *in vivo* opportunities.